Supporting Information for:

Structure of Choline Chloride-Carboxylic Acid Deep Eutectic Solvents by Wide-Angle X-ray Scattering and DFT Calculations

Keke Chai[a, e], Yongquan Zhou[*a, c], Xingmei Lu[b, c], Toshio Yamaguchi [a], Koji Ohara[d], Hongyan Liu[a], Fayan Zhu[a]

[a]Key Laboratory of Comprehensive and Highly Efficient Utilization of Salt Lake Resources; Key Laboratory of Salt Lake Resources Chemistry of Qinghai Province; Qinghai Institute of Salt Lakes, Chinese Academy of Sciences, Xining, Qinghai 810008, China

[b]Beijing Key Laboratory of Ionic Liquids Clean Process, CAS Key Laboratory of Green Process and Engineering, Institute of Process Engineering, Chinese Academy of Sciences, 100190 Beijing, China.

[c]Innovation Academy for Green Manufacture, Chinese Academy of Sciences, 100190 Beijing, China.

[d]Diffraction and Scattering Division, Japan Synchrotron Radiation Research Institute, 1-1-1 Kouto, Sayo, Hyogo 679-5198, Japan.

[e]University of Chinese Academy of Sciences, Beijing 100049, China.

*All correspondence should be sent to: Prof. Yongquan Zhou, E-mail: yongqzhou@ 163.com.

The detailed information of reference 38:

Frisch, M. J.; Trucks, G. W.; Schlegel, H. B.; Scuseria, G. E.; Robb, M. A.; Cheeseman, J. R.; Scalmani, G.; Barone, V.; Petersson, G. A.; Nakatsuji, H.; Li, X.; Caricato, M.; Marenich, A. V.; Bloino, J.; Janesko, B. G.; Gomperts, R.; Mennucci, B.; Hratchian, H. P.; Ortiz, J. V.; Izmaylov, A. F.; Sonnenberg, J. L.; Williams; Ding, F.; Lipparini, F.; Egidi, F.; Goings, J.; Peng, B.; Petrone, A.; Henderson, T.; Ranasinghe, D.; Zakrzewski, V. G.; Gao, J.; Rega, N.; Zheng, G.; Liang, W.; Hada, M.; Ehara, M.; Toyota, K.; Fukuda, R.; Hasegawa, J.; Ishida, M.; Nakajima, T.; Honda, Y.; Kitao, O.; Nakai, H.; Vreven, T.; Throssell, K.; Montgomery Jr., J. A.; Peralta, J. E.; Ogliaro, F.; Bearpark, M. J.; Heyd, J. J.; Brothers, E. N.; Kudin, K. N.; Staroverov, V. N.; Keith, T. A.; Kobayashi, R.; Normand, J.; Raghavachari, K.; Rendell, A. P.; Burant, J. C.; Iyengar, S. S.; Tomasi, J.; Cossi, M.; Millam, J. M.; Klene, M.; Adamo, C.; Cammi, R.; Ochterski, J. W.; Martin, R. L.; Morokuma, K.; Farkas, O.; Foresman, J. B.; Fox, D. J. Gaussian 16 Rev. A.03, Wallingford, CT, 2016.

Wide-angle X-ray scattering data treatments

The experimental scattering intensities of sample solutions and an empty capillary were corrected for absorption. Then, the scattering intensities of sample solutions were obtained by subtracting the corrected intensity of the empty capillary. After absorption correction and empty capillary subtraction, the scattering intensities were normalized to electron units by comparing the asymptote of the scattering intensities with the calculated coherent intensities and incoherent intensities at large scattering vector (Q > 15 Å^{-1}). The normalization factor was re-checked by Krogh-Moe and Norman integration methods. [1, 2] The normalization factors by the two methods agreed with each other within

2%. The structural function $I^{coh}(Q)$ of each solution was calculated by subtracting the independent scatterings, which is the sum of incoherent and coherent scattering of all atoms in the solution from the normalized intensity as Eq. (S1)

$$I^{coh}(Q) = KI_p(Q) - \sum_{i=1}^{N_{atom}} x_i\left[f_i^2(Q) + (\Delta f_i^{''})^2 + I_i^{incoh}(Q)\right] \quad \text{(S1)}$$

The Q-weighted structure function $Q{\cdot}I(Q)$ was Fourier-transformed to the radial distribution function (RDF) by Eq. (S2)

$$G(r) = 4\pi r^2\rho_0 + \frac{2r}{\pi}\int_0^{Q_{max}} Q \cdot I(Q) \cdot M(Q) \cdot \frac{sin(Qr)}{Qr} dQ \quad \text{(S2)}$$

where r is radial distance. ρ_0 stands for the average electron number density of the sample solutions ($\rho_0 = \left[\sum_{i=1}^{N_{atom}} n_i f_i(0)\right]^2 \Big/ V$), *i.e.*, average electron scattering ability when the scattering angle of the sample is 0 ($e^2{\cdot}Å^{-3}$). $f_i(0)$, atomic scattering factor of the i-th atom with Q = 0. Q_{max} is the upper limit of Q available in the experiments. The modification function $M(Q)$ is defined as Eq. (S3)

$$M(Q) = \left\{\sum_{i=1}^{N_{atom}} n_i\left[f_i^2(0) + \left(\Delta f_i^{''}\right)^2\right] \Big/ \sum_{i=1}^{N_{atom}} n_i\left[f_i^2(Q) + \left(\Delta f_i^{''}\right)^2\right]\right\} \cdot exp(-k{\cdot}Q^2) \quad \text{(S3)}$$

here, the k (damping factor) is 0.01 $Å^2$ to reduce the influence of experimental error and integral truncation error, and is also to suppress the sharpening effect caused by the first term. The spurious peaks are removed by peak shape calculation and second Fourier transform. By calculating the theoretical peak of the intramolecular interactions within a water molecule and performing Fourier inverse transformation in the usual manner, [3] the spurious ripples below 1 $Å^{-1}$ were removed from RDF.

All corrections and treatments of scattering data were performed with the KURVLR program. [4]

EPSR adopts Monte Carlo to make the theoretical structure factor close to that of the experiment by randomly moving atomic positions. The experimental total normalized structure factor used in EPSR is defined as Eq. (S4)

$$F^{exp}(Q) = \frac{\left[I^{coh}(Q) - \sum n_i f_i^2(Q)\right]}{[\sum n_i f_i^2(Q)]} \tag{S4}$$

The theoretical $F^{sim}(Q)$ is calculated by Eq. (S5) and compared with the experimental $F^{exp}(Q)$.

$$F^{sim}(Q) = \sum_i \sum_{j \geq i} (2 - \delta_{ij}) c_j f_i(Q) f_j(Q) \cdot [A_{ij}(Q) - 1] / [\sum c_i f_i^2(Q)] \tag{S5}$$

$$A_{ij}(Q) - 1 = 4\pi\rho \int_0^\infty r^2 (g_{ij}(r) - 1) \frac{sinQr}{Qr} dQ \tag{S6}$$

here, c_i and c_j are the atomic fractions of atom types i and j, $f_i(Q)$ and $f_j(Q)$ are the Q dependent atomic scattering factors of atom types i and j, δ_{ij} is the Kronecker function to avoid double counting pairs of atoms of the same type, $A_{ij}(Q)$ is the Faber-Ziman partial structure factor, $g_{ij}(r)$ is the pair distribution functions of all atoms existing in the sample.

The total radial distribution functions, $G(r)$, is calculated as Eq. (S7)

$$G(r) = \sum_i \sum_{j \geq i} (2 - \delta_{ij}) c_j f_i(Q) f_j(Q) (g_{ij}(r) - 1) \tag{S7}$$

The initial structure of EPSR simulation is generated by putting an appropriate number of ions and molecules into a box to obtain the required density. The potential energy of the simulation box is calculated as Eq. (S8) and (S9)

$$U_{tot} = U_{intra} + \sum_i \left(4\varepsilon_{ij} [(\frac{\sigma_{ij}}{r_{ij}})^{12} - (\frac{\sigma_{ij}}{r_{ij}})^6] + \frac{q_i q_j}{4\pi\varepsilon_0 r_{ij}} \right) + U_{EP} \tag{S8}$$

$$\varepsilon_{ij} = (\varepsilon_i \varepsilon_j)^{\frac{1}{2}}, \ \sigma_{ij} = \frac{1}{2}(\sigma_i + \sigma_j) \tag{S9}$$

here, U_{intra} is described by using a series of harmonic potentials, ε_{ij} and σ_{ij} are the Lennard-Jones parameters for the potential well depth and effective atom size, respectively. ε_0 is the vacuum

permittivity, r_{ij} is the interatomic spacing, q_i is the atomic charge, U_{EP} is the empirical potential generated by EPSR, [5-7] which is purely obtained by fitting the simulation results with the experimental scattering data. This empirical potential term can make the simulated structure factor as close to the experimental scattering data as possible without violating the atomic overlap, van der Waals force and hydrogen bond.

Table S1. EPSR simulation setup details.

No.	Ch^+	Cl^-	FA/AA	*Density*/ atoms Å^{-3}	*Box side Length*/ Å	Iterations times
ChFA	250	250	500	0.09604	43.6730	20000
ChAA	250	250	500	0.09721	46.0615	20000

Table S2. Potential parameter values for EPSR modelling [8-10] (the charge of FA/AA are RESP charge)

atom type	ε /kJ • mol^{-1}	σ /Å	*Mass*/amu	q/e
N	0.7000	3.200	14.0067	-0.604000
CMT	0.8000	3.700	12.0111	-0.349000
C2N	0.8000	3.700	12.0111	-0.099000
HMT	0.2000	2.580	1.00800	0.250000
HCN	0.2000	2.580	1.00800	0.250000
COH	0.8000	3.700	12.0111	0.050000
HCO	0.2000	2.580	1.00800	0.090000
OH	0.6500	3.100	15.9994	-0.650000
HOH	0.0000	0.000	1.00800	0.420000
Cl	0.5660	4.191	35.4529	-1.00000
CF	0.4393	3.750	12.0111	0.586502
HF	0.2000	2.580	1.00800	0.061180
OCF	0.6500	3.100	15.9994	-0.514882
OF	0.6500	3.100	15.9994	-0.571063
HOF	0.0000	0.000	1.00800	0.438263
CTA	0.7000	3.200	12.0111	-0.433884
HMA	0.2000	2.580	1.00800	0.092500
HCA	0.2000	2.580	1.00800	0.163178
COA	0.4393	3.750	12.0111	0.758027

OCA	0.6500	3.100	15.9994	-0.560468
OA	0.6500	3.100	15.9994	-0.597951
HOA	0.0000	0.000	1.00800	0.415393

DFT calculations

Table S3. The structural and energy parameters of ChFA and ChAA

	ChFA-GA	ChFA-GB	ChFA-TA		ChAA-GA	ChAA-GB	ChAA-TA
N···Cl	4.03 Å	4.42 Å	3.74 Å	N···Cl	4.07 Å	4.01 Å	3.77 Å
HMT···Cl	2.59 Å	2.95 Å	2.53 Å	HMT···Cl	3.01 Å	2.58 Å	2.60 Å
HOH···Cl	2.25 Å	4.25 Å	-	HOH···Cl	4.90 Å	2.24 Å	-
HMT···OCF	2.77 Å	2.64 Å	2.65 Å	HMT···OCA	2.60 Å	2.50 Å	2.56 Å
HCN···OCF	3.79 Å	2.31 Å	2.30 Å	HOH···OCA	1.80 Å	4.11 Å	2.06 Å
Cl···OCF	3.83 Å	3.71 Å	3.69 Å	Cl···OCA	3.68 Å	3.83 Å	3.85 Å
Cl···OF	3.06 Å	2.99 Å	2.91 Å	Cl···OA	2.99 Å	3.07 Å	2.94 Å
Cl···HOF	2.07 Å	1.99 Å	1.88 Å	Cl···HOA	1.99 Å	2.09	1.93 Å
ΔE (kcal·mol^{-1})	-121.63	-120.32	-111.18	ΔE (kcal·mol^{-1})	-123.92	-120.83	-115.07

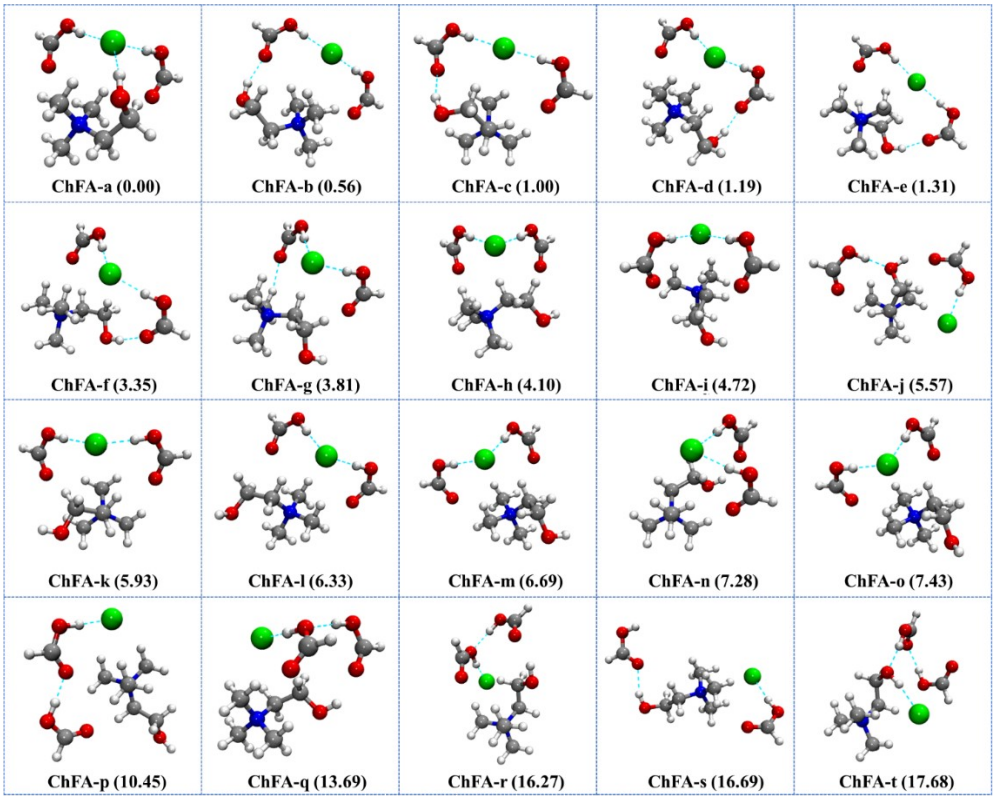

Fig 1S Typical optimized structures of ChFA (relative energy, kcal·mol^{-1}) at ωB97XD/6-311++G(d,p) basis level

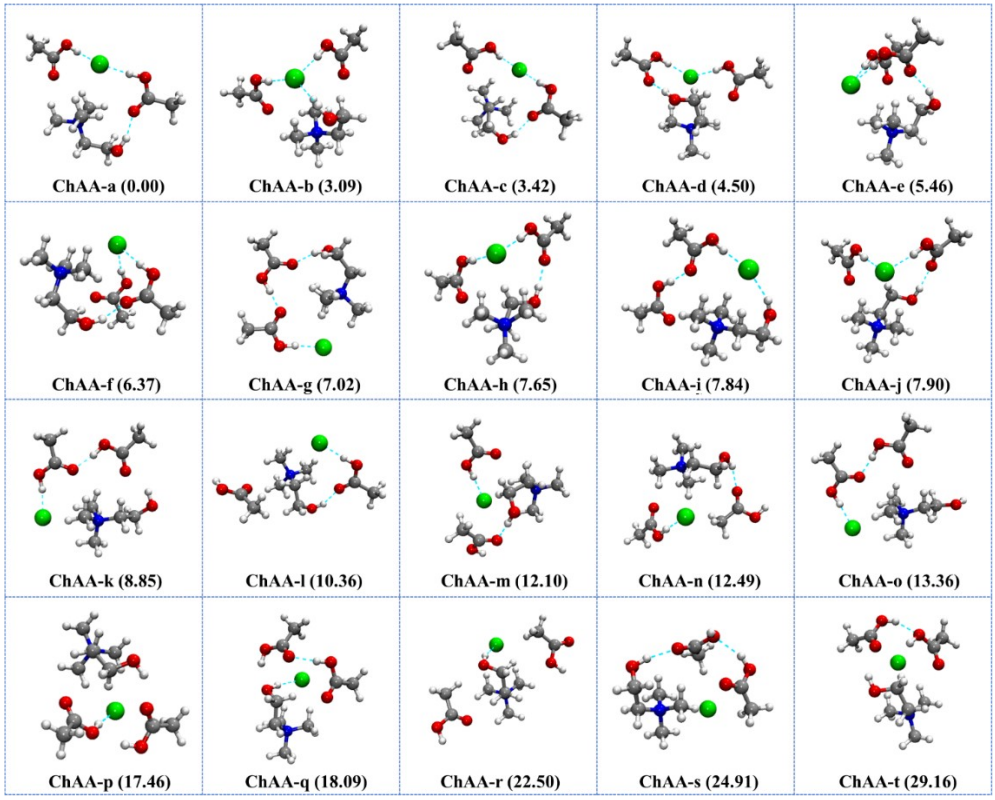

Fig 2S Typical optimized structures of ChAA (relative energy, kcal·mol^{-1}) at ωB97XD/6-311++G(d,p) basis level

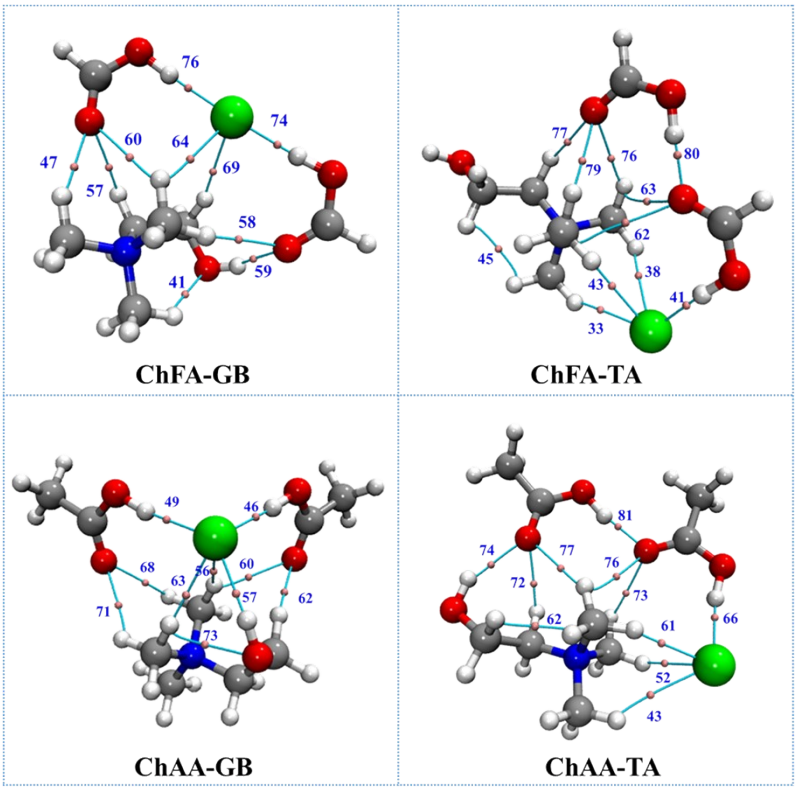

Fig. 3S. Bond paths and bond critical points (BCP) of ChFA-GB, ChFA-TA, ChAA-GB and ChAA-TA.

Table S4 Analysis of the bond critical points in ChFA-GA (all values in a.u.)

BCP	Hydrogen bond	$\rho(r)$	$\nabla^2\rho(r)$	λ_1	λ_2	λ_3
47	Cl···HOF	0.0320	0.0721	-0.0415	0.1549	-0.0413
66	Cl···HOF	0.0331	0.0730	-0.0433	0.1593	-0.0431
57	HMT···Cl	0.0124	0.0374	0.0578	-0.0103	-0.0101
58	HMT···Cl	0.0126	0.0372	-0.0103	-0.0104	0.0579
67	HOH···Cl	0.0226	0.0648	0.1144	-0.0245	-0.0252
72	HCN···OCF	0.0123	0.0395	-0.0124	-0.0118	0.0637
36	HMT···OCF	0.0111	0.0393	0.0590	-0.0091	-0.0106
37	HMT···OCF	0.0114	0.0404	-0.0111	0.0612	-0.0097
63	HMT···OCF	0.0091	0.0320	-0.0076	0.0452	-0.0056
60	HMT···OH	0.0117	0.0416	-0.0063	0.0576	-0.0098

Table S5 Analysis of the bond critical points in ChFA-GB (all values in a.u.)

BCP	Hydrogen bond	$\rho(r)$	$\nabla^2\rho(r)$	λ_1	λ_2	λ_3
74	Cl···HOF	0.0184	0.0621	-0.0190	-0.0198	0.1008

76	Cl···HOF	0.0380	0.0750	0.1790	-0.0521	-0.0518
64	HMT···Cl	0.0115	0.0366	-0.0081	0.0539	-0.0092
69	HCO···Cl	0.0130	0.0386	-0.0113	0.0610	-0.0111
57	HCN···OCF	0.0121	0.0420	-0.0114	0.0651	-0.0117
47	HMT···OCF	0.0153	0.0615	-0.0156	0.0936	-0.0164
60	HMT···OCF	0.0075	0.0244	0.0369	-0.0060	-0.0065
58	HMT···OCF	0.0107	0.0349	0.0555	-0.0105	-0.0101
59	HOH···OCF	0.0270	0.1133	-0.0363	-0.0375	0.1872
41	HMT···OH	0.0184	0.0621	-0.0190	-0.0198	0.1008

Table S6 Analysis of the bond critical points in ChFA-TA (all values in a.u.)

BCP	Hydrogen bond	$\rho(r)$	$\nabla^2\rho(r)$	λ_1	λ_2	λ_3
41	Cl···HOF	0.0529	0.0640	-0.0805	0.2246	-0.0801
33	HMT···Cl	0.0147	0.0443	0.0702	-0.0129	-0.0130
38	HMT···Cl	0.0140	0.0415	0.0653	-0.0121	-0.0117
43	HMT···Cl	0.0142	0.0421	0.0664	-0.0123	-0.0120
78	HCN···OCF	0.0116	0.0442	-0.0106	0.0662	-0.0114
76	HMT···OCF	0.0091	0.0282	-0.0080	0.0440	-0.0079
79	HMT···OCF	0.0119	0.0385	-0.0116	0.0615	-0.0114
63	HMT···OCF	0.0068	0.0255	0.0342	-0.0031	-0.0055
80	HOF···OCF	0.0518	0.1483	-0.0955	0.3369	-0.0931

Table S7 Analysis of the bond critical points in ChAA-GA (all values in a.u.)

BCP	Hydrogen bond	$\rho(r)$	$\nabla^2\rho(r)$	λ_1	λ_2	λ_3
43	Cl···HOA	0.0417	0.0734	0.1910	-0.0590	-0.0586
47	Cl···HOA	0.0364	0.0748	0.1730	-0.0493	-0.0490
52	HMT···Cl	0.0108	0.0343	-0.0074	0.0502	-0.0085
55	HMT···Cl	0.0084	0.0264	-0.0043	0.0366	-0.0058
71	HMT···OCA	0.0128	0.0423	0.0675	-0.0125	-0.0127
79	HMT···OCA	0.0151	0.0610	-0.0154	0.0923	-0.0159
57	HMT···OCA	0.0122	0.0399	0.0637	-0.0121	-0.0117
54	HMT···OCA	0.0107	0.0359	-0.0095	0.0556	-0.0101
58	HOH···OCA	0.0328	0.1275	-0.0468	0.2234	-0.0490
69	HMT···OH	0.0106	0.0370	0.0522	-0.0063	-0.0089

Table S8 Analysis of the bond critical points in ChAA-GB (all values in a.u.)

BCP	Hydrogen bond	$\rho(r)$	$\nabla^2\rho(r)$	λ_1	λ_2	λ_3
46	Cl···HOA	0.0318	0.0726	0.1543	-0.0410	-0.0408

49	Cl···HOA	0.0301	0.0712	0.1476	-0.0383	-0.0381
57	HOH···Cl	0.0232	0.0656	-0.0253	0.1168	-0.0260
56	HMT···Cl	0.0127	0.0376	-0.0105	-0.0105	0.0586
63	HMT···Cl	0.0131	0.0395	-0.0111	0.0615	-0.0109
60	HMT···OCA	0.0096	0.0339	0.0481	-0.0082	-0.0061
68	HMT···OCA	0.0121	0.0429	0.0653	-0.0119	-0.0104
71	HMT···OCA	0.0117	0.0418	-0.0098	0.0629	-0.0113
62	HCO···OCA	0.0130	0.0422	-0.0126	0.0682	-0.0133

Table S9 Analysis of the bond critical points in ChAA-TA (all values in a.u.)

BCP	Hydrogen bond	$\rho(r)$	$\nabla^2\rho(r)$	λ_1	λ_2	λ_3
66	Cl···HOA	0.0469	0.0664	-0.0685	0.2030	-0.0681
43	HMT···Cl	0.0067	0.0181	0.0256	-0.0036	-0.0039
52	HMT···Cl	0.0180	0.0543	0.0880	-0.0170	-0.0167
61	HMT···Cl	0.0183	0.0545	0.0893	-0.0173	-0.0176
73	HMT···OCA	0.0109	0.0364	-0.0105	0.0563	-0.0094
76	HMT···OCA	-0.0105	0.0386	-0.0068	0.0549	-0.0095
77	HMT···OCA	0.0099	0.0304	0.0485	-0.0089	-0.0092
72	HCN···OCA	0.0141	0.0527	-0.0136	0.0796	-0.0133
74	HOH···OCA	0.0186	0.0707	-0.0217	0.1145	-0.0221
81	HOA···OCA	0.0490	0.1427	0.3164	-0.0881	-0.0856

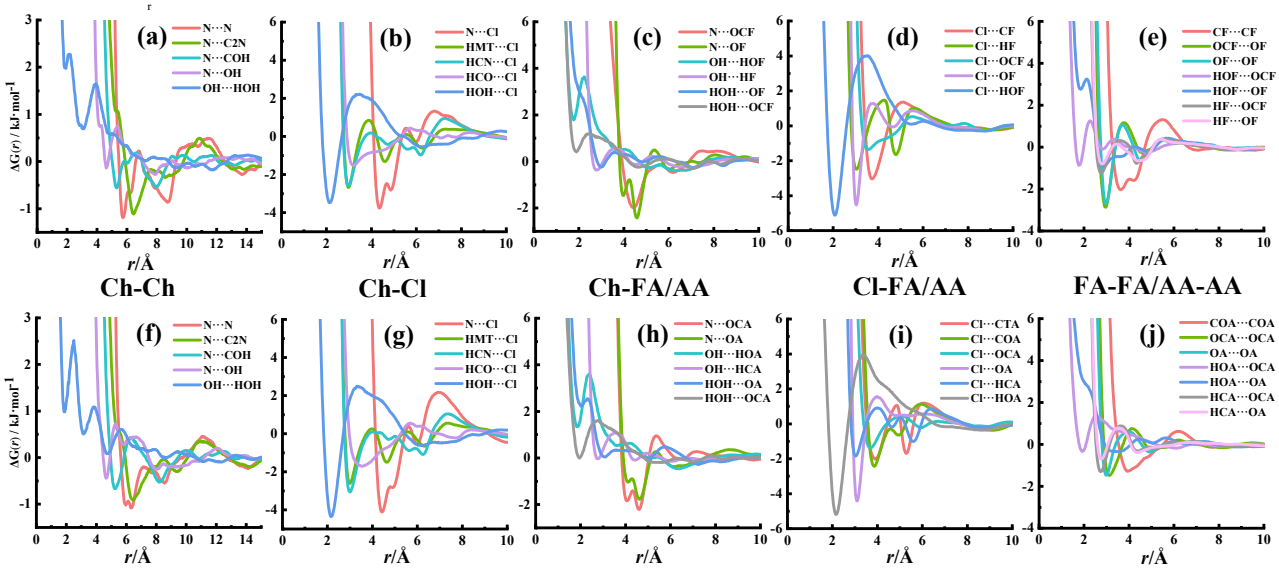

Fig. 4S The potentials of mean force of ChClFA (top panel) and ChClAA (bottom panel).

1. N. Norman, *Acta Cryst*, 1957, **10**, 370-373.

2. J. Krogh-Moe, *Acta Cryst*, 1956, **9**, 951-953.

3. R. Kaplow, S. L. Strong and B. L. J. P. R. Averbach, *American Physical Society*, 1965, **138**, A1336-A1345.

4. G. Johanson and M. Sandstörm, *Chemica. Scripta.*, 1973, **4**, 195-198.

5. S. J. L. Billinge and M. F. Thorpe, 2002.

6. A. K. Soper, *Chem. Phys.*, 1996, **202**, 295-306.

7. A. K. Soper, *Phys. Rev. B*, 2005, **72**, 104204.

8. O. S. Hammond, D. T. Bowron and K. J. Edler, *Green. Chem.*, 2016, **18**, 2736-2744.

9. S. Fathi, M. A. Gonzalez, M. Bahri, S. Nasr and M.-C. Bellissent-Funel, *J. Mol. Liq.*, 2015, **207**, 125-135.

10. D. Lengvinaitė, K. Aidas and L. Kimtys, *Phys. Chem. Chem. Phys.*, 2019, **21**, 14811-14820.